Available online at www.sciencedirect.com
ScienceDirect
Journal of the European Ceramic Society 29 (2009) 2003–2011
www.elsevier.com/locate/jeurceramsoc

Combustion synthesis and characterization of LSCF-based materials as cathode of intermediate temperature solid oxide fuel cells

Atanu Dutta, Jayanta Mukhopadhyay, R.N. Basu *

Fuel Cell & Battery Division, Central Glass & Ceramic Research Institute, Council of Scientific & Industrial Research (CSIR), 196, Raja S.C. Mullick Road, Kolkata 700032, India

Received 22 July 2008; received in revised form 7 November 2008; accepted 18 November 2008
Available online 3 January 2009

Abstract

Nanocrystalline SOFC cathode materials of perovskite family, $La_{1-x}Sr_xM_{1-y}Co_yO_3$, where $0<x\leq 0.5$, $0<y\leq 0.8$ (M is transitional metal = Mn or Fe), have been synthesized at a relatively low temperature by combustion synthesis using alanine as a novel fuel. Detailed X-ray powder diffraction analyses show 47–96% phase purity in the as-synthesized powder and upon calcination at ~825 °C single-phase material is obtained wherein the nanocrystallinity (crystallite size ~19–24 nm) is retained. Densification studies of the materials are carried out within 900–1100 °C. The coefficient of thermal expansion (CTE) of these cathodes is measured. Electrical conductivity of the cathodes sintered at different temperatures are measured in the temperature range 700–900 °C and correlated with the density of the sintered materials. The electrochemical performances of Ni-YSZ anode-supported SOFC having YSZ electrolyte (~10 μm) with CGO interlayer (~15 μm) are studied with the developed cathodes in the temperature range 700–800 °C using H_2 as fuel and oxygen as oxidant. Highest current density of ~1.7 A/cm^2 is achieved during testing at 800 °C measured at 0.7 V with a cathode composition of $La_{0.5}Sr_{0.5}Co_{0.8}Fe_{0.2}O_3$. Precipitation of nanocrystalline grains over the core grains in porous microstructure of this cathode might be one of the reasons for such high cell performance.

Keywords: Anode-supported SOFC; Nanocrystalline; LSCF cathode; CGO interlayer

1. Introduction

For the state-of-the-art anode-supported SOFC operating at ~800 °C, the conventional $La_{1-x}Sr_xMnO_{3-\delta}$ (LSM)-based cathode is not showing satisfactory performance due to sluggish oxygen reduction reaction (ORR) kinetics which causes low current drawing capacity of the cell.[1] Moreover, the polarization loss at the cathode further increases when the operating temperature of SOFC single cells is below 800 °C.[2] Hence, considerable efforts are being made to develop new class of perovskite-based cathode materials with high electrocatalytic activity for oxygen reduction at a relatively lower operating temperature of SOFC (700–800 °C). For this purpose, several new compositions showing mixed ionic and electronic conductivity (MIEC) have been investigated as promising SOFC cathodes.[1–11] Amongst these, the perovskite-based compounds having the general formula $La_{1-x}Sr_xM_{1-y}Co_yO_3$, where $0<x\leq 0.5$ and $0<y\leq 0.8$ (M is a transitional metal, Mn or Fe) has found significant attention[5–11] because of their superior MIEC behavior[5–8] as well as enhanced ORR kinetics.[9–15] The La(Sr)Co(Fe) (LSCF)-based cathodes, in particular, are reported to be very effective for IT-SOFC (700–800 °C) application when coupled with a Gd-doped ceria (CGO)-based interlayer.[5,6,11,12] This is mainly due to high ionic conductivity in CGO electrolyte, compared to conventional 8 mol% yittria-stabilized zirconia (8-YSZ) together with its favorable coefficient of thermal expansion (CTE). While the CTE values of YSZ and CGO electrolytes are 10.8×10^{-6} K^{-1} and 12.8×10^{-6} K^{-1}, respectively, for LSCF-based cathodes it is found to be much higher ($>17\times10^{-6}$ K^{-1}).[6] Hence a CGO interlayer is considered as buffer to reduce the mechanical stresses at the interfaces.[5,6] Another significance of using CGO is to prevent the undesirable reactions between LSCF-based cathodes with YSZ electrolyte during high temperature processing,[5,6] otherwise, resistive phases like $La_2Zr_2O_7$ and $SrZrO_3$ are formed at the interface which in turn reduces the cell performance drastically.

Depending on the synthesis and processing, the nanocrystalline nature of LSCF-based cathode enhances the electro-

* Corresponding author. Tel.: +91 33 24733469; fax: +91 33 24730957.
E-mail addresses: rnbasu@cgcri.res.in, rajenbasu@yahoo.ca (R.N. Basu).

0955-2219/$ – see front matter © 2008 Elsevier Ltd. All rights reserved.
doi:10.1016/j.jeurceramsoc.2008.11.011

catalytic reduction of oxidant along with higher catalytic activity because of extremely high surface area.[15] In addition, nanocrystalline cathodes are easily sinterable and the extent of sinterability of these powders can be tailor made by addition of requisite amount of organic vehicle and binder during preparation of thick film paste for screen printing. In the present work, three different LSCF-based nanocrystalline cathodes, e.g., $La_{0.8}Sr_{0.2}FeO_3$ (LS2), $La_{0.8}Sr_{0.2}Co_{0.8}Fe_{0.2}O_3$ (LS3) and $La_{0.5}Sr_{0.5}Co_{0.8}Fe_{0.2}O_3$ (LS4) are prepared by combustion synthesis technique.[16] Conventional cathode (LSM) having composition $La_{0.65}Sr_{0.3}MnO_3$ (LS1)[17,18] is also synthesized by the same technique for comparison of electrochemical performances. The LSCF-based cathode materials thus synthesized are characterized for structural, thermal and electrical properties and compared with conventional LSM cathode. Finally, the electrochemical performances of Ni-YSZ/YSZ (∼10 μm) anode-supported single cells are evaluated with these cathode materials using CGO as an interlayer. The CGO thus used is prepared in-house using combustion synthesized technique.

2. Experimental

The synthesis procedure adopted for all the four compositions (LS1, LS2, LS3 and LS4) is similar and is schematically shown in Fig. 1. The starting materials used for the synthesis of the cathode batches are stoichiometric amount of lanthanum (III) nitrate hexahydrate (99%, Sisco Res. Lab. Ltd., India), strontium (II) nitrate (99%, s.d.fine, India), manganese (II) acetate tetrahydrate (99.5%, E. Merck, Germany), iron (III) nitrate nonahydrate (Across Chemicals) and cobalt (II) nitrate hexahydrate (99.5%, E. Merck, Germany) using a saturated aqueous solution of alanine as a fuel (99%, Qualigens, India). First, a saturated aqueous solution of stoichiometric amounts of the respective metal nitrates and acetates are mixed and stirred on a hot plate at ∼150 °C. A saturated aqueous solution of alanine (99%, Qualigens, India) is added to these solution mixtures, keeping same mole ratio of alanine to nitric acid (alanine:nitrate = 1:1) in order to maintain proper fuel-to-oxidant ratio and to control the undesired hydrolysis of the respective precursor salts. After vigorous stirring, the whole solution is turned into a viscous gel. An instantaneous burning of those gels produces ash. The as-synthesized powders (ash) are then calcined at 700 °C and 825 °C for 4 h in air. The significance of alanine as a novel fuel in the combustion synthesis process has already been reported by our group.[16] The viscous gels of all the samples are collected for thermal analysis. The differential thermal analysis (DTA) and thermogravimetric analysis (TGA) are carried out from room temperature to 800 °C in air at a heating rate of 10 °C/min using Shimadzu TA-50 Thermal Analyzer. X-ray diffractograms are recorded by a Philips X'pert X-ray diffractometer with a CuKα radiation at 40 kV and 40 mA. The X-ray data are collected in the 2θ range 10–80° with a scan rate of 0.5°/min and a dwell time of 0.02 s. Rietveld refinement of the powder diffraction profiles and quantitative phase analysis are done using a pseudovoight function by PANalytical Highscore Plus software. Size–strain analysis is performed by comparing the particle width of a standard silicon scan to account for the instrument broadening. Field emission scanning electron microscopy (FESEM, Gemini Supra 35 Zeiss) and scanning electron microscope (Leo S430i) are used to examine the morphology of the powders and microstructures of the sintered samples. For the densification studies, powders calcined at 825 °C are pressed uniaxially with a specific pressure of 170 MPa and subsequently the green samples are sintered in the temperature range of 900–1100 °C for 4 h in air. The sintered density of all the samples is determined by standard Archimedes principle. The CTE of the relatively highest and lowest dense sintered samples is measured by a dilatometer (NETZSCH, DIL 402) up to 800 °C with a constant heating rate of 10 °C/min.

The electrical conductivity of the sintered samples (900–1100 °C) is measured in the temperature range 700–900 °C in air by 4-probe technique using a Power Source (Agilent E3631A) and a Multimeter (Keithley 2002). The data is registered in every 25 °C interval. Platinum paste is used as current collecting electrode on either side of the sintered pellet and the electrode is cured at 950 °C for 2 h before the electrical conductivity measurement. Planar anode-supported single cells of configuration NiO-YSZ/YSZ/CGO/LSCF-based cathodes with ∼10 μm YSZ electrolyte and 1.5 mm cermet anode are fabricated using CGO as an interlayer. The CGO thus used is prepared in-house using combustion synthesized technique. The details of NiO-YSZ/YSZ half cell fabrication by tape casting is reported elsewhere.[18] The CGO thick film paste is screen printed over sintered YSZ electrolyte of NiO-YSZ/YSZ half cell and sintered in

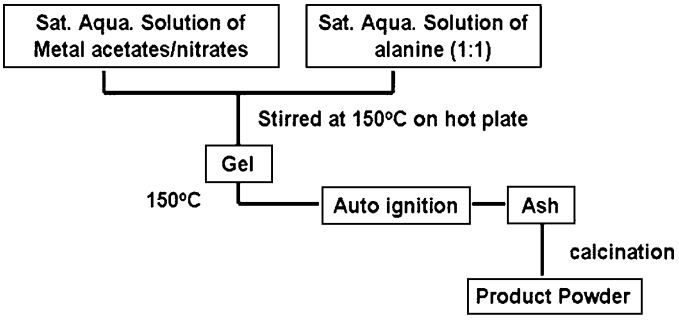

Fig. 1. Flow diagram for alanine assisted combustion synthesis of cathode materials.

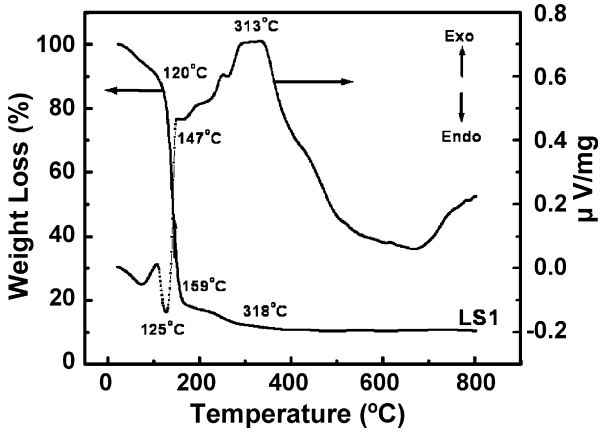

Fig. 2. TG/DTA analysis of LSM gel in the temperature range of 30–800 °C.

the temperature range between 1100 °C and 1350 °C. The thick film paste of the synthesized cathode material is further screen printed over the sintered CGO layer and subsequently fired at 1100 °C for 4 h to prepare single cells with all the four cathodes. The electrochemical measurements of such single cells are carried out in the form of coupon cells (16 mm diameter, 1.5 mm thick with active cathode area of ~0.3 cm^2) in the temperature range 700–800 °C using an in-house electrochemical measurement setup. Moist H_2 (~3% H_2O) is used as a fuel on the anode side and oxygen is fed on the cathode side. During the measurement, the flow rates for both the fuel and O_2 are maintained at 100 SCCM (standard cubic centimeter).

3. Results and discussion

3.1. Powder characterization

Fig. 2 shows the thermal analysis of the precursor gel of LS1 in the temperature range 30–800 °C. The endothermic peak observed at 125 °C in the DTA curve is due to the evaporation of water. A drastic weight loss in the TG curve occurs at ~159 °C and the corresponding exothermic peak at 147 °C in the DTA indicates a sharp, single-step decomposition of lanthanum–alanine and manganese–alanine complexes. The X-ray diffractograms of the LSM powders (LS1) calcined at 700 °C and 825 °C, respectively are shown in Fig. 3. Analysis of the as-synthesized powder shows a phase purity of about 50% along with considerable amounts of $LaMnO_3$ and Mn_3O_4 as secondary phases. After calcination at 700 °C, the phase purity improves to ~90%. However, upon calcinations at 825 °C, a single-phase rhombohedral of $La_{0.65}Sr_{0.3}MnO_3$ is obtained. All the peaks have been identified with the standard JCPDS file number 50-0308. The calculated lattice parameters as obtained are $a = b = 5.467$ Å and $c = 13.494$ Å. The average crystallite size is found to be 16 nm and 23 nm for the powders calcined at 700 °C and 825 °C, respectively. The TGA and DTA (inset) plots of the LS2–LS4 gels in the temperature range 30–800 °C is shown in Fig. 4. The thermal behavior of all the three LSCF-based

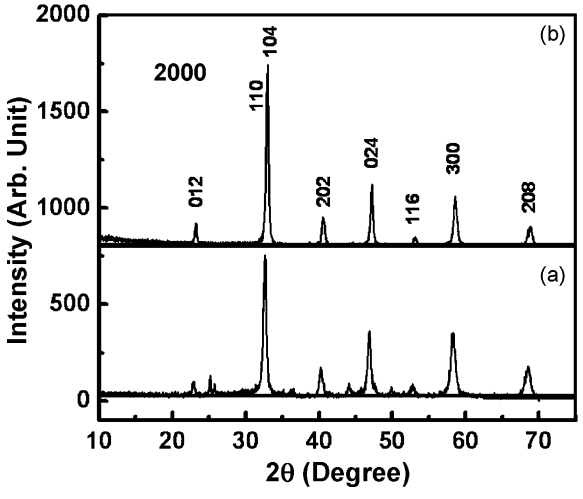

Fig. 3. X-ray diffractograms of LS1 powders calcined at (a) 700 °C and (b) 825 °C.

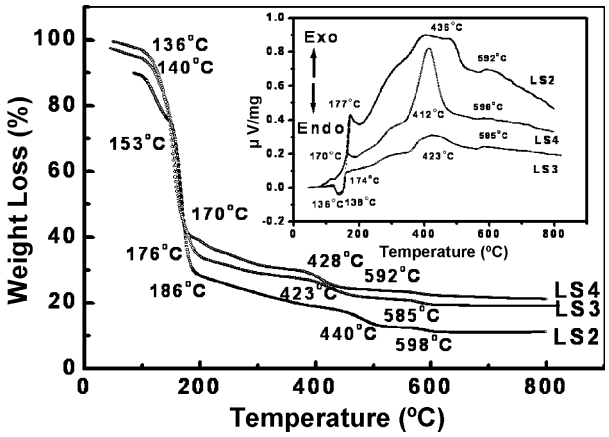

Fig. 4. TG/DTA analysis of various LSCF gels in the temperature range of 30–800 °C.

gels (LS2–LS4) is found to be similar in nature. After an initial small weight loss at ~140 °C, a major and sharp weight loss occurs below 200 °C indicating decomposition of metal complexes and formation of crystalline phase of the powder. Corresponding XRD patterns of the various LSCF-based powders calcined at 825 °C are shown in Fig. 5. Phase analysis of the diffractograms reveals that LS2 consists of a predominantly rhombohedral phase, together with an orthorhombic phase. On the other hand, for LS3, on substitution of Fe with Co, the structure becomes completely rhombohedral with no other secondary phase. However, for LS4, presence of a small amount of La_2O_3 is also observed along with the rhombohedral phase. For all these materials a phase purity of ~96% is achieved in the as-synthesized conditions and 100% phase purity is reached after calcining all the powders at 700 °C. But in order to compare the crystallite size with LS1 (Fig. 3), the calcination temperature for these powders is maintained to 825 °C. The average crystallite sizes of all the LSCF-based cathode materials thus obtained after calcinations are found to be 23 nm, 24 nm and 19 nm corresponding to LS2–LS4 powders, respectively. The powder morphology of all the cathode powders investigated (calcined at 700 °C) reveal agglomerated nature

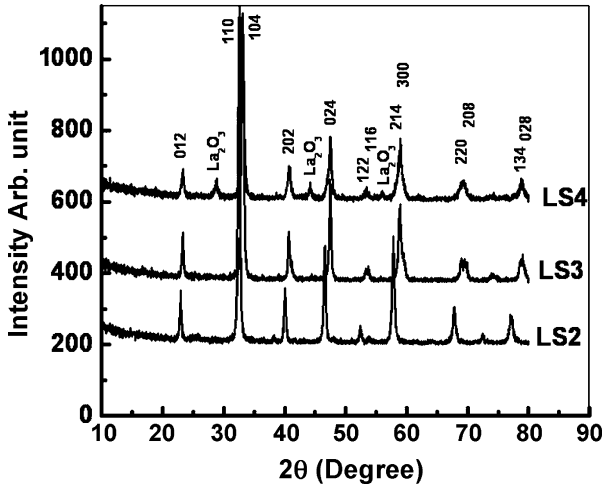

Fig. 5. X-ray diffractograms of LS2–S4 powders calcined at 825 °C.

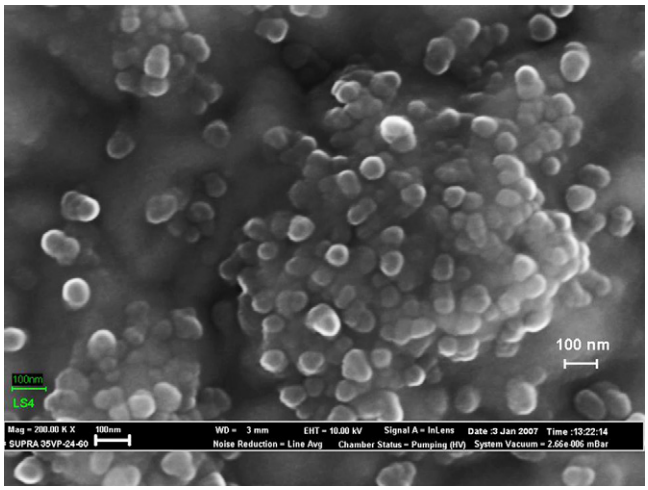

Fig. 6. Field emission scanning electron micrograph of $La_{0.5}Sr_{0.5}Co_{0.8}Fe_{0.2}$ (LS4) powder calcined at 700 °C.

of the particles with an estimated size of ~50 nm. In particular, some distinct agglomerate free particulates are observed in case of LS4 powder (Fig. 6) in comparison with other powders.

3.2. Densification and thermal expansion studies

Density of the studied cathode materials is systematically evaluated for different sintering temperatures to find its influence on the electrical conductivity. However, it is true that while applied as cathode in SOFC material has to be porous in nature. The influence of sintering temperature on percentage theoretical density is shown in Fig. 7. The theoretical density of the prepared cathodes, e.g., LS1–LS4 are evaluated from the X-ray diffraction data. The sintered densities are found to increase for all the samples with the increase in sintering temperature. It is observed that in general the sintered density is relatively low for LS1 compared to LS2–LS4. However, among the LSCF-based cathodes, LS3 shows a maximum densification at around 1000 °C after which

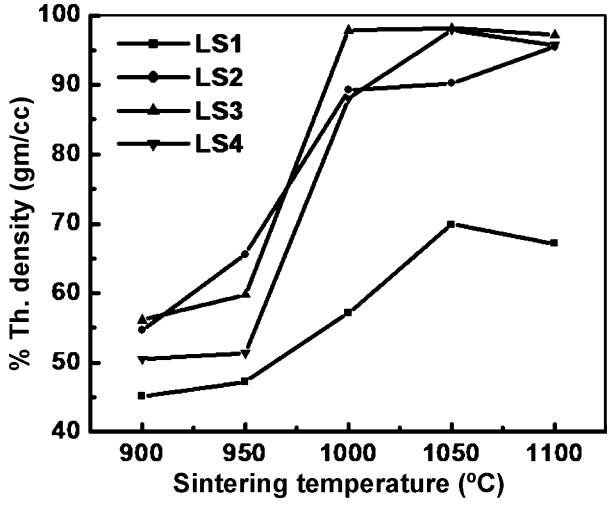

Fig. 7. Variation of percentage theoretical density with sintering temperatures.

Table 1
Coefficients of thermal expansion (CTE) of synthesized cathodes measured at 800 °C.

Cathodes	LS1	LS2	LS3	LS4
CTE ($\times 10^{-6}$) K^{-1} (sintered at 900 °C)	12.99	10.11	19.26	18.31
CTE ($\times 10^{-6}$) K^{-1} (sintered at 1100 °C)	13.05	12.11	19.32	19.23

it remains almost constant. On the other hand, in case of LS4, an intermediate trend of rise in density up to a temperature 1000 °C is observed and maximum density is reached at ~1050 °C. For LS4, the decrease in density is very marginal when the sintering temperature is increased from 1050 °C to 1100 °C. In this system, higher level of La substitution by Sr in the A-site results in higher solute drag which normally occurs because of the strong interaction between segregated and the grain boundary elements. As the grain growth mobility is inversely proportional to the segregated concentration of the elements, therefore, higher level of segregated elements results in slow grain boundary mobility.[19] At 1100 °C, this retards necessary intergranular pore elimination process resulting in marginal decrease in the percentage of densification although the grain growth is almost complete. The detailed correlation of the sintered density with the microstructures and electrical conductivity is discussed in the subsequent section.

Coefficients of thermal expansion of all these cathodes measured from room temperature up to 800 °C are given in Table 1. The CTE values obtained are quite high (>18 × 10^{-6} K^{-1}) for cobalt containing samples (LS3 and LS4) which is not compatible with other SOFC cell components. Similar kind of CTE values are also reported in the literature for these materials.[6] On the other hand, for LS1 and LS2, the obtained CTE values (11–13 × 10^{-6} K^{-1}) are comparable with that of the other cell components. Although CTE is primarily the property of material but based on the composition of the material and degree of substitution, the value of CTE may be influenced by the sintering temperature which we have observed in the case of LS2 and LS4. In particular, higher level of Sr substitution in the A-site of LS4 cathode might have some role in addition to cobalt in the sintering behavior and hence the CTE value changes upon sintering in the temperature range of 900–1100 °C. To understand this behavior more systematic study is required. Because of relatively high values of CTEs for LS3 and LS4, single cells fabricated with these cathodes often exhibit micro-cracks at the cathode side even if the sintering schedule is controlled appropriately. However, detailed investigation reveals that the CTEs as obtained in combination of these cathode materials and ceria-based interlayer are more compatible to the other SOFC cell components.[20] Hence, electrochemical investigations of the anode-supported single cells using these types of cathodes (LS3 and LS4) are done with doped ceria as an interlayer in between the cathode and the YSZ electrolyte. Sintering of such single cells using ceria-based interlayer do not show any micro-cracks at the cathode surface or at cathode/interlayer/YSZ interfaces which implies that this interlayer compensates the mismatch of CTE for these cathodes (LS3 and LS4) with YSZ electrolyte.[5]

3.3. Microstructural studies

SEM studies reveal that the densification increases with the sintering temperature for all the cathode materials which is in accordance with the results of the densification studies as described before. Fig. 8 shows the SEM micrographs of fractured surface of LS4, LS3, LS2 and LS1 cathode sintered at 1100 °C. Again, from Fig. 7 it is clear that LS1 does not densify effectively even at 1100 °C compared to other cathodes under investigation. Strontium-doped lanthanum ferrite (LS2) shows better sinterability than LS1 at 1100 °C, yet the sintered grains are not clearly visible. On the other hand, strontium and cobalt-doped lanthanum ferrites (LS3 and LS4) show prominent sintered grains with distinct grain boundaries when sintered at 1050 °C and 1100 °C. Quite interestingly, in case of LS4 having more Sr doping in A-site than LS3, some nanocrystalline grains are found to be uniformly precipitated within the core grains that starts at sintering temperature 1050 °C and becomes more prominent at 1100 °C. However, this phenomenon is not observed in case of LS3 when sintered in the same temperature range (1050–1100 °C). Presence of cobalt and iron helps in the sintering process of LSCF system and probably due to liquid phase sintering high densification is achieved at temperature as low as 1050 °C. It is believed that the precipitation of nanocrystalline grains at the time of recrystallization is only observed for heavy A-site (Sr) doping in LS4 system ($La_{0.5}Sr_{0.5}Co_{0.8}Fe_{0.2}O_3$) only. After recrystallization of the nano-grains within the large size core gains, grain coarsening starts which results in low sintered density around 1100 °C.

3.4. Electrical conductivity and electrochemical performance evaluations

The perovskite structures ($ABO_{3-\delta}$) doped with transition metal oxides of Fe, Co, Mn, etc. are well known for their MIEC properties.[5] All the synthesized cathodes, e.g., LS1–LS4 prepared under different sintering conditions are used for electrical conductivity measurement. Fig. 9 shows $\ln(\sigma T)$ vs. $1/T$ plot indicating the influence of sintering temperature on the temperature-dependent electrical conductivity behavior for the samples measured within the range between 700 °C and 900 °C. In general, it can be seen that the electrical conductivity is very low for all the samples when sintered at or below 950 °C. It can be seen from the plots that none of the cathode materials show Arrhenius type linear behavior of conductivity with respect to measuring temperature when sintered below 1000 °C.

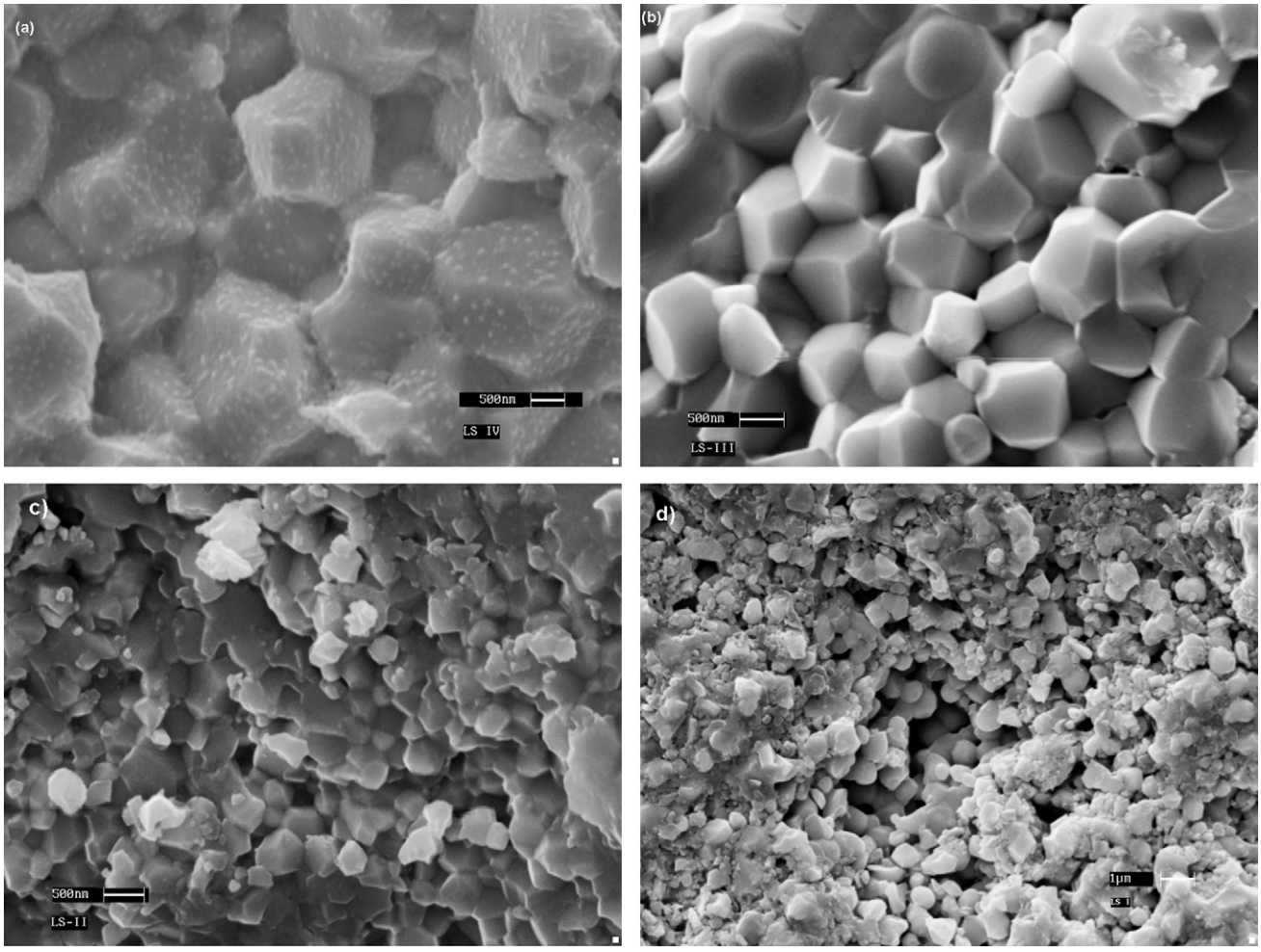

Fig. 8. Fracture surface micrographs of (a) LS4, (b) LS3, (c) LS2 and (d) LS1 cathodes sintered at 1100 °C.

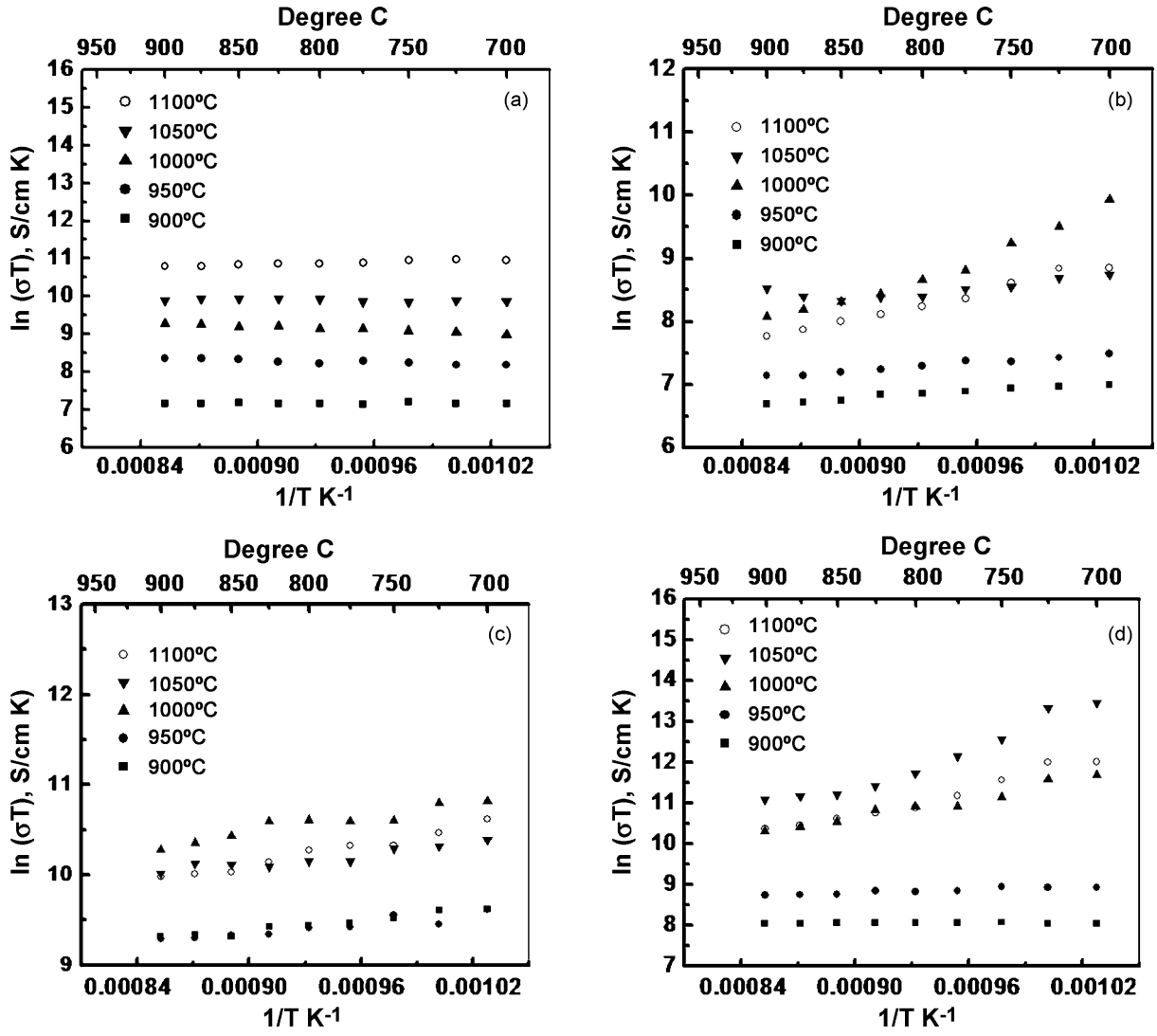

Fig. 9. ln(σT) vs. 1/T plots for (a) LS1, (b) LS2, (c) LS3 and (d) LS4 cathode compositions at five sintering temperatures (900–100 °C).

On the other hand, at sintering temperature of 1000 °C and above the conductivity decreases with the increase of temperature for LS2–LS4 and metal-like linear behavior of conductivity change with temperature is clearly evident. The typical activation energy of conduction for LS4 however is found to be in the range 0.1–1.2 eV. For LS1, the electrical conductivity showing metal-like behavior gives relatively higher values only when sintered at 1100 °C. The reason for low conductivity in LS1 is presumably due to low density and insignificant increase of densification with the increase of sintering temperature. The increase in conductivity value with decrease in measurement temperature is sluggish for both LS2 and LS3 for all the sintering temperatures. In contrast, for LS4 the conductivity value decreases significantly from 714 S/cm at 700 °C to 115 S/cm at 800 °C for samples sintered at 1050 °C. Incidentally, highest sintered density is obtained for LS4 at 1050 °C. As for comparison, the electrical conductivity value measured at 800 °C (σ_{800}) for LS4, LS3, LS2 and LS1 are 115 S/cm, 24 S/cm, 4 S/cm, 19 S/cm and 60 S/cm, 26 S/cm, 4 S/cm, 40 S/cm when sintered at 1050 °C and 1100 °C, respectively. Tai et al.[21] and Stevenson et al.[22] showed that in case of LSCF with low Fe content, the nature of conductivity is predominantly metallic rather than semiconducting.

Fig. 10 shows single-cell performance with current–voltage (*I–V*) and current–power (*I–P*) characteristics having LSCF-based cathodes (LS4 and LS3). In these cells, CGO interlayer is sintered at ~1300 °C. It can be seen that while cell with LS4 cathode produces a current density as high as ~1.72 A/cm^2, the cell based on LS3 cathode produces only 0.62 A/cm^2 when measured at 800 °C under cell operating voltage of 0.7 V. A comparison of electrochemical performances of all cathodes investigated in this study is shown in Table 2. The difference of performance can be considered primarily due to electrocatalytic activity of each of the cathodes. Microstructures of all the studied cathodes are analyzed after the single-cell testing. It appears from the micrographs that LS3 cathode is much denser than LS4. From the densification study (Fig. 7) it is also observed that density of LS3 is higher than LS4 at sintering temperature of 1100 °C. Thus the low porosity at the LS3 cathode could be responsible for low electrochemical performance.

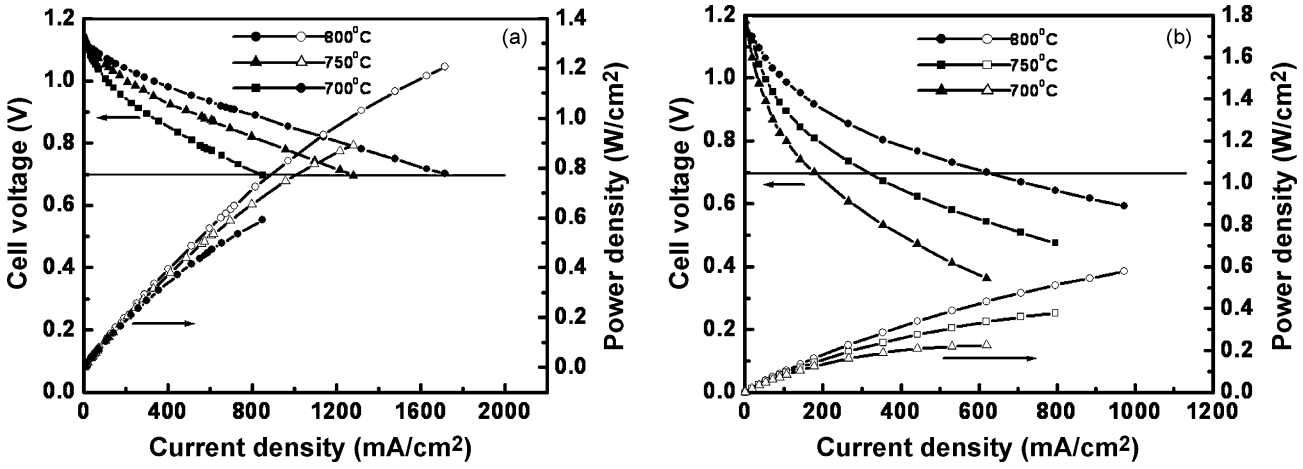

Fig. 10. Electrochemical cell performance of anode-supported single cell with CGO as interlayer for (a) LS4 and (b) LS1 cathodes.

Table 2
Electrochemical properties of the anode-supported cells with developed cathodes.

Cathode	Current density (A/cm^2) at 0.7 V			ASR (Ω cm^2) at 800 °C
	800 °C	750 °C	700 °C	
LS4	1.720	1.280	0.849	0.211
LS3	0.619	0.320	0.185	0.339
LS2	0.029	0.015	0.009	7.61
LS1	0.165	0.092	0.040	2.85

It is also evident in the present work that the performance of LSF-based cathode is inferior to LSM-based cathode. However, it is observed that when LSF cathode is sintered at 1150 °C, the single-cell performance improves and a current density of ~0.4 A/cm^2 could be achieved at 0.7 V for operating temperature 800 °C. The reason for poor performance for LSF-based cathode when sintered at 1100 °C in the present work could be due to excessive porosity of the cathode layer surface which might improve upon sintering at 1150 °C. Though the sintered density of the bulk sample of LSF is found to be higher than that of LSM (Fig. 7), but the screen printed layer of such LSF-based cathode on to sintered CGO interlayer might have different densification behavior. Since the detailed optimization of sintering temperature of all the studied cathodes and their microstructures are beyond the scope of the present manuscript, these data are not included.

Fig. 11(a) shows the SEM microstructure of top surface of LS4 cathode after the cell test. Precipitation of nanocrystalline grains over relatively bigger grains is clearly observed. Similar observation is also made in the dense microstructure of LS4 cathode (Fig. 8a). However, both in dense and porous microstructure of LS3 cathode, such nanocrystaline grains are not observed when sintered at 1100 °C. It is anticipated that probably these nanocrystalline grains enhance the electrochemical reaction on the LS4 cathode surface because of the enhancement of the total three-phase boundary (TPB) length near the nanocrystalline precipitates. Of course, the interface of CGO-based interlayer and LS4-based cathode is crucial for the electrochemical performance of the single cells. Micrograph of polished cross-section of single cell is analyzed, nanocrystalline precipitates could also be observed at the LS4 region of the interface with CGO interlayer although not very clearly. Fig. 11(b) shows the cross-section of the single cell with LS4 cathode after cell test, wherein the inset shows a magnified view of LS4 near the interface. Thus, the phenomenon of increased surface area on the LS4 surface near the interface due to nanocrystalline precipitates also exists.

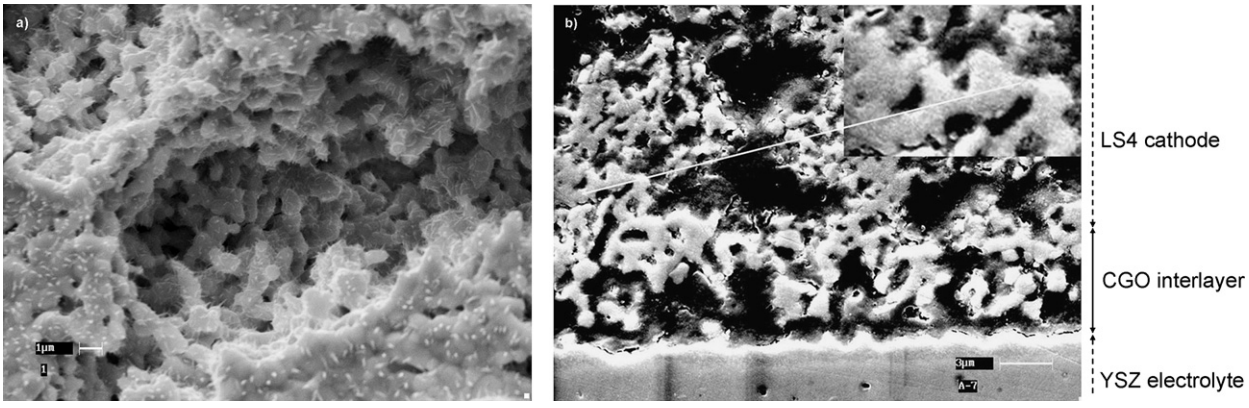

Fig. 11. SEM microstructure of (a) the top layer of $La_{0.5}Sr_{0.5}Co_{0.8}Fe_{0.2}$ (LS4) cathode and (b) corresponding fractured anode-supported single cell with CGO as interlayer after the cell test.

It is reported that the optimum sintering temperature for LSCF-based cathodes may vary with the composition to obtain best cell performance.[23] However, in the present work, at the same sintering temperature of 1100 °C the electrochemical performance of the developed cathodes is compared and it is observed that LS4 cathode produces much higher current drawing capacity in the single cell with respect to the other cathodes. Kim et al.[24] pointed out that the current density dependent total area-specific resistance (ASR) of the cell can be calculated from the linear portion of the current–voltage characteristics corresponding to the cell voltage from 1.0 V to 0.7 V. In addition to ohmic contributions from electrolyte, electrodes and the corresponding interfaces, polarization resistances at the electrode–electrolyte interface also contribute towards the total ASR value of the cell. The evaluated ASR value of single cells with different cathodes is presented in Table 2. While the ASR for cell with LS4 cathode is found to be lowest (0.211 $\Omega\,cm^2$), the same are relatively higher for other cathodes. The ASR value estimated for LS4 cathode in the present work is similar to the value reported by Mai et al.[5] Therefore, it can be concluded that in the anode-supported single cell with Gd-doped ceria interlayer, $La_{0.5}Sr_{0.5}Co_{0.8}Fe_{0.2}O_3$ (LS4) cathode having highest electrical conductivity and unique microstructure results in superior electrochemical performance compared to the results obtained with other cathodes.

4. Conclusions

Nanocrystalline powders (~20 nm) of LSM and LSCF-based cathode materials have been prepared successfully by combustion synthesis technique using alanine as a novel fuel. This fuel induces a sharp single-step combustion at a low temperature (<200 °C) which results up to 96% of phase purity in the as-synthesized powder as evident from the XRD analysis. The powders are agglomerated in nature (average size ~50 nm). However, all the powders except lanthanum strontium manganite (LS1) are found to be highly sinteractive. Highest densification for $La_{0.8}Sr_{0.2}Co_{0.8}Fe_{0.2}O_3$ (LS3) and $La_{0.5}Sr_{0.5}Co_{0.8}Fe_{0.2}O_3$ (LS4) are obtained for samples sintered at 1000 °C and 1050 °C, respectively. In the measured temperature range (700–900 °C), the electrical conductivity is found to be metal-like in nature. The change of electrical conductivity with temperature is much more pronounced for LS4 and it shows the highest electrical conductivity. The electrochemical performance of YSZ-based planar SOFC with CGO interlayer is found to vary with the composition of the developed cathodes. Highest current density of ~1.72 A/cm^2 and power density of 1.2 W/cm^2 at 0.7 V, operating at 800 °C is obtained with $La_{0.5}Sr_{0.5}$ $Co_{0.8}Fe_{0.2}O_3$ (LS4) as the cathode in anode-supported cell having CGO as the interlayer. Lowest value of total ASR is observed (~0.211 $\Omega\,cm^2$) with LS4 cathode only. It is evident from the microstructural analysis that the small nanocrystalline growth inside the core grains might play a crucial role on the electrochemical performances of the developed anode-supported single cells.

Acknowledgements

The authors acknowledge CSIR-NMITLI project for financial support and Director, CGCRI for his kind permission to publish this work. Technical assistance from X-ray and SEM Divisions of the Institute is also acknowledged.

References

1. Jiang, S. P., A comparison of O_2 reduction reactions on porous (La,Sr)MnO_3 and (La,Sr)(Co,Fe)O_3 electrodes. *Solid State Ionics*, 2002, **146**, 1–22.
2. Jørgensen, M. J. and Mogensen, M., Impedance of solid oxide fuel cell LSM/YSZ composite cathodes. *J. Electrochem. Soc.*, 2001, **148**, A433–A442.
3. Dusastre, V. and Kilner, J. A., Optimisation of composite cathodes for intermediate temperature SOFC applications. *Solid State Ionics*, 1999, **126**, 163–174.
4. Kusščer, D., Holc, J., Hrovat, S. and Kolar, D., Correlation between the defect structure, conductivity and chemical stability of $La_{1-y}Sr_yFe_{1-x}Al_xO_{3-\delta}$ cathodes for SOFC. *J. Eur. Ceram. Soc.*, 2001, **21**, 1817–1820.
5. Mai, A., Haanappel, V. A. C., Uhlenbruck, S., Tietz, F. and Stöver, D., Ferrite-based perovskites as cathode materials for anode-supported solid oxide fuel cells. Part I. Variation of composition. *Solid State Ionics*, 2005, **176**, 1341–1350.
6. Mai, A., Haanappel, V. A. C., Tietz, F. and Stöver, D., Ferrite-based perovskites as cathode materials for anode-supported solid oxide fuel cells. Part II. Influence of the CGO interlayer. *Solid State Ionics*, 2006, **177**, 2103–2107.
7. Teraoka, Y., Zhang, H. M., Okamoto, K. and Yamazoe, N., Mixed ionic-electronic conductivity of $La_{1-x}Sr_xCo_{1-y}Fe_yO_{3-\delta}$ perovskite-type oxides. *Mater. Res. Bull.*, 1988, **23**, 51–58.
8. Fleig, J., On the width of the electrochemically active region in mixed conducting solid oxide fuel cell cathode. *J. Power Sources*, 2002, **105**, 228–238.
9. Adler, S. B., Lane, J. A. and Steele, B. C. H., Electrode kinetics of porous mixed-conducting oxygen electrode. *J. Electrochem. Soc.*, 1996, **143**, 3554–3564.
10. Kilner, J. A., De Souza, R. A. and Fullarton, I. C., Surface exchange of oxygen in mixed conducting perovskite oxide. *Solid State Ionics*, 1996, **86–88**, 703–709.
11. Fleig, J., Solid oxide fuel cell cathodes: polarization mechanisms and modeling of the electrochemical performance. *Annu. Rev. Mater. Res.*, 2003, **33**, 361–382.
12. Adler, S. B., Factors governing oxygen reduction in solid oxide fuel cell cathode. *Chem. Rev.*, 2004, **104**, 4791–4844.
13. Tanasescu, S., Totir, N. D. and Marchidan, D. I., Thermodynamic properties of some perovskite type oxides used as SOFC cathode material. *Solid State Ionics*, 1999, **119**, 311–315.
14. Holc, J., Kusščer, D., Hrovat, M., Bernik, S. and Kolar, D., Electrical and microstructural characterisation of $(La_{0.8}Sr_{0.2})(Fe_{1-x}Al_x)O_3$ and $(La_{0.8}Sr_{0.2})(Mn_{1-x}Al_x)O_3$ as possible SOFC cathode materials. *Solid State Ionics*, 1997, **95**, 259–268.
15. Taniguchi, I., Landschoot, R. C. and Schoonman, J., Fabrication of $La_{1-x}Sr_xCo_{1-y}Fe_yO_3$ thin films by electrostatic spray deposition. *Solid State Ionics*, 2003, **156**, 1–13.
16. Raja, M. W., Mahanty, S., Ghosh, P., Basu, R. N. and Maiti, H. S., Alanine-assisted low-temperature combustion synthesis of nanocrystalline $LiMn_2O_4$ for lithium-ion batteries. *Mater. Res. Bull.*, 2007, **42**, 1499–1506.
17. Basu, R. N., *Materials for Solid Oxide Fuel Cells in Recent Trends in Fuel Cell Science and Technology*. Jointly published by Anamaya Publisher and Springer, New Delhi (India) and New York, 2006 [Chapter 12], pp. 284–329.
18. Basu, R. N., Sharma, A. D., Dutta, A. and Mukhopadhyay, J., Processing of high performance anode-supported planar solid oxide fuel cell. *Int. J. Hydrogen Energy*, 2008, **33**, 5748–5754.
19. Chiang, Y. M., Birnie III, D. and Kingery, W. D., Physical ceramics, principles for ceramics and engineering. In *MIT Series in Materials Science & Engineering*, ed. C. Robichand and K. Santor. John Wiley and Sons, New York, NJ, 1996 [Chapter 5], pp. 351–428.

20. Tsoga, A., Gupta, A., Naoumidis, A. and Nikolopoulos, P., Gadolinia-doped ceria and yttria stabilized zirconia interfaces: regarding their application for SOFC technology. *Acta Mater.*, 2000, **48**, 4709–4714.
21. Tai, L. W., Nasrallah, M. M., Anderson, H. U., Sparlin, D. M. and Sehlin, S. R., Structure and electrical properties of $La_{1-x}Sr_xCo_{1-y}Fe_yO_3$. Part 1. The system $La_{0.8}Sr_{0.2}Co_{1-y}Fe_yO_3$. *Solid State Ionics*, 1995, **76**, 259–271.
22. Stevenson, J. W., Armstrong, T. R., Carneim, R. D., Pederson, L. R. and Weber, W. J., Electrochemical properties of mixed conducting perovskites $La_{1-x}M_xCo_{1-y}Fe_yO_{3-\delta}$ (M = Sr, Ba, Ca). *J. Electrochem. Soc.*, 1996, **143**(9), 2722–2729.
23. Tietz, F., Haanappel, V. A. C., Mai, A., Mertens, J. and Stöver, D., Performance of LSCF cathodes in cell tests. *J. Power Sources*, 2006, **156**, 20–22.
24. Kim, J. W., Virkar, A. V., Fung, K. Z., Mehta, K. and Singhal, S. C., Polarization effects in intermediate temperature, anode-supported solid oxide fuel cells. *J. Electrochem. Soc.*, 1999, **146**(1), 69–78.